

Numerical analysis of a new SMA-based seismic damper system and material characterization of two commercial NiTi-alloys

J. S. Olsen*

Norwegian University of Science and Technology, 7491 Trondheim, Norway

C. Van der Eijk‡

SINTEF Materials and Chemistry, 7465 Trondheim, Norway

Z. L. Zhang*†

Norwegian University of Science and Technology, 7491 Trondheim, Norway

(Received March 1, 2007, Accepted September 1, 2007)

Abstract. The work presented in this paper includes material characterisation and an investigation of suitability in seismic dampers for two commercially available NiTi-alloys, along with a numerical analysis of a new damper system employing composite NiTi-wires. Numerical simulations of the new damper system are conducted, using Brinson's one-dimensional constitutive model for shape memory alloys, with emphasis on the system's energy dissipation capabilities. The two alloys tested showed some unwanted residual strain at temperatures higher than A_s , possibly due to stress concentrations near inclusions in the material. These findings show that the alloys are not ideal, but may be employed in a seismic damper if precautions are made. The numerical investigations indicate that using composite NiTi-wires in a seismic damper enhances the energy dissipation capabilities for a wider working temperature range.

Keywords: shape memory alloys; NiTi; seismic damper; pseudoelasticity; WIND-CHIME; numerical simulation; design principles; residual strain; one-dimensional constitutive model; parameter study.

1. Introduction

The work presented in this paper is a part of the EU 6th frame STREP project WIND-CHIME, which aims to develop cost effective seismic dampers to protect historical monuments during earthquakes. The structures in question are often located in areas that experience large shifts in temperature, demanding the dampers to perform optimal within a wide working temperature range.

*E-mail: Jim.Stian.Olsen@ntnu.no

‡E-mail: casper.v.eijk@sintef.no

††Corresponding Author, E-mail: Zhiliang.Zhang@ntnu.no

In the recent years increasing attention has been given to the use of shape memory alloys (SMAs) as members in seismic control schemes (Saadat, *et al.* 2002, Janke, *et al.* 2005). In particular, research considering the NiTi-alloy as an actuator in seismic control devices has received attention due to the materials unique thermomechanical properties. One example of this is the EU project MANSIDE, which resulted in a seismic damper for civil structures and bridges (Dolce, *et al.* 2001).

NiTi has received this attention because of its unusual properties shape memory effect (SME) and pseudelasticity (PE). SME is the ability of the material to recover to its predetermined shape after being subjected to large deformation (ca. 8%) (Funakubo 1987, Duerig 1990). The recovery is induced by heating the material above a threshold temperature. PE represents SMA's ability to recover from large deformations purely by unloading. Both SME and PE are the results of diffusionless phase transformations in the material induced by temperature variation and stress. At temperatures above the threshold temperature A_f (austenite finishing temperature), the structure of the material is 100% austenite. If it is subjected to sufficient stress, martensite will gradually develop until the material structure is 100% martensitic. Martensite created in this way is often referred to as stress induced remove paragraph insertion martensite (SIM). The material will return to the austenite phase when unloaded (Funakubo 1987, Duerig 1990). By subjecting SIM to additional stress it will continue to deform elastically before plastic deformation is developed due to dislocations. If the material is cooled below the threshold temperature M_s (martensite starting temperature) from an initial austenite phase, martensite will gradually develop as the temperature is reduced. The structure will be 100% martensitic when the ambient temperature sinks below the threshold temperature M_f (martensite finishing temperature). This is called thermally induced martensite (TIM). For a more detailed review of the characteristics and accelerations in SMA research, reference are made to the book by Auricchio, *et al.* (2001).

Most seismic dampers found in the literature are designed to function at practically constant temperature (Clark, *et al.* 1995, Dolce, *et al.* 2001, Han, *et al.* 2005). Little emphasis has been put on control schemes that focus on the challenges with changing working temperatures. In this paper, two commercially available NiTi-alloys are characterised and tested for suitability in seismic devices. In addition, design principles for a new damper system are proposed and investigated numerically. The objective of the system is to effectively perform as an energy dissipation device when subjected to load in an environment with varying temperatures. To accomplish this multiple NiTi-wires of different alloys will be employed in a damper. Different NiTi-Alloys exhibit optimal energy dissipation capabilities at different temperatures. By taking advantage of this, the general idea is to optimize the damper dissipation capacity for the entire working temperature range. The work presented cover material testing of commercially available NiTi-Alloys and numerical analysis of the new damper system.

2. Characteristics of commercially available NiTi-alloys

In order to get a realistic view of the new damper systems performance, a series of investigations on commercially available NiTi-alloys were conducted to obtain metallurgical and mechanical characteristics. Two NiTi-alloys, designated AF5 and AF30, were chosen based on threshold temperatures and expected

Table 1 Chemical composition of the two NiTi-alloys, at %

	Ni	Ti	C
AF5	50.0	49.7	0.27
AF30	49.2	50.6	0.27

Table 2 Phase transformation temperatures of the as-received and heat treated materials

	A_s	A_f	R'_s	R'_f	M_s	M_f	R_s	R_f
AF5, as-received	-60°C	-33°C			-72°C			
AF5, 575°C, 1 hr.	-5°C	4°C			-40°C	-52°C	-9°C	-23°C
AF30, as-received	-60°C	-37°C			-71°C	-92°C		
AF30, 450°C, 1 hr.	30°C	41°C	16°C	27°C	-53°C	-67°C	43°C	24°C

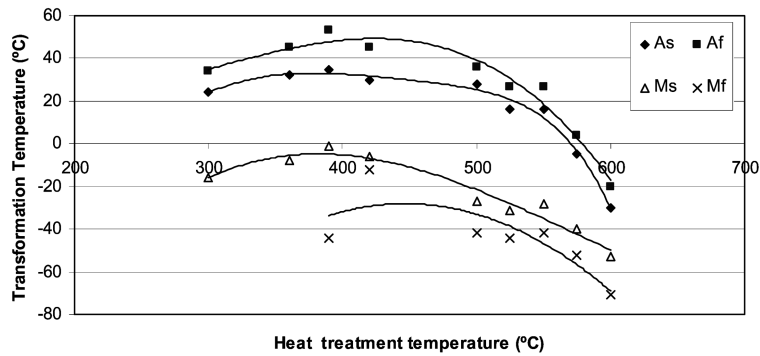


Fig. 1 Transformation curves as a function of the heat treatment (1hr, air cooled) temperature for the AF5 material

behaviour accordingly. Table 1 shows the chemical compound of the materials.

The alloys were heat treated in order to influence the phase transformation temperatures and ensure presence of the pseudoelastic effect at room temperature. The AF5 and AF30 materials were heat treated at 575 °C and 450 °C for one hour respectively and air-cooled. DSC measurements were performed to establish phase transformation temperatures. Table 2 shows these temperatures, here R_s and R_f denotes transformation start and finish temperatures for the R-phase. Fig. 1 shows the dependence of the phase transformation temperatures as function of the heat treatment temperatures for the AF5 material.

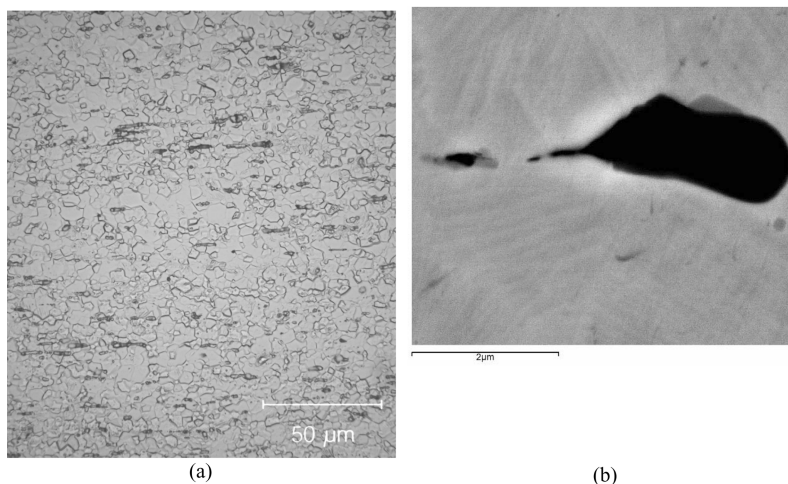


Fig. 2 (a) Microstructure of the AF5 material. (b) SEM backscattered image showing a Ti-carbide inclusion in the AF5 material

2.1. Metallurgical characteristics

Investigation by Optical Microscopy, of the as-received materials, reveals a very fine microstructure with a typical grain size of less than 10 μm for both the AF5 and AF30 materials. The microstructure of the AF5 material is shown in Fig. 2(a). A large number of second phase particles (inclusions) with elongated morphology are present in both materials. These observations are confirmed by Scanning Electron Microscopy (SEM) investigations. A SEM backscattered image shows the inclusions in the AF5 material in Fig. 2(b). By performing EDS analyses it is established that the inclusions are generally Ti-carbides. These may be recognized by their gold-like colour.

Size distribution of the second phase articles is established by an Automatic Image analysis. The sizes of the measured surfaces are 6 mm^2 and 0.26 mm^2 at 40 and 500 times magnification respectively. Due to the stretched morphology both minimum and maximum diameter are measured. The investigations show an average size in the elongated direction of 1.9 μm , and 0.9 μm in the transverse direction. The inclusion density is measured to be on average 5500/ mm^2 . The two alloys exhibit approximately the same inclusion characteristics.

2.2. Mechanical characteristics

The mechanical characteristics were investigated by performing tensile tests at various temperatures. The tests were conducted with a servo hydraulic tensile testing machine, and the specimen temperature controlled with a heat chamber capable of temperatures in the range -150 $^{\circ}\text{C}$ -250 $^{\circ}\text{C}$. Displacement was registered using an extensometer. The length of the specimen wires were 200 mm, and the diameter 2 mm. Several testing procedures were performed to capture the material behaviour in a best possible manner:

- 1) Loading and unloading with a maximum elongation of 5% in the temperature range -10-70 $^{\circ}\text{C}$ with temperature steps of 10 $^{\circ}\text{C}$.
- 2) Cyclic testing with varying amplitude at a temperature where the material showed a closed stress-strain loop. Specimen wires in this procedure were subjected to 10 training cycles prior to testing.
- 3) Loading and unloading with a maximum elongation of 7% in a temperature range covering all threshold temperatures of the materials. This was conducted to establish parameters for numerical analyses.

The first two procedures were performed with a sinus shaped strain control with a frequency of 0.02 Hz, while the last procedure was performed with strain controlled ramping at 100 mm/min. The wires were slightly pre-tensioned to avoid initial buckling of the wires.

2.2.1. Testing results

Fig. 3 shows the stress-strain curves for the AF5 and AF30 materials. For temperatures lower than A_f (4 $^{\circ}\text{C}$ and 41 $^{\circ}\text{C}$ for the AF5 and AF30 materials respectively), a residual strain is present, the residual strain is decreasing as the temperature increases towards A_f . This is due to retained martensite in the material, and may be eliminated by heating. The AF5 material exhibits the lowest residual strain at 10 $^{\circ}\text{C}$, while the AF30 material does so at 40 $^{\circ}\text{C}$. At temperatures higher than A_f , the residual strain increases for both materials. The critical transformation stresses increases approximately linear throughout the temperature range with the exception of a drop at 70 $^{\circ}\text{C}$ for the AF5 material. This decrease indicates that the working temperature has exceeded M_D . M_D is the temperature where plastic deformation takes place before martensite development.

Fig. 4 shows the cyclic stress-strain curves for the AF5 and AF30 materials at varying strain amplitude. The

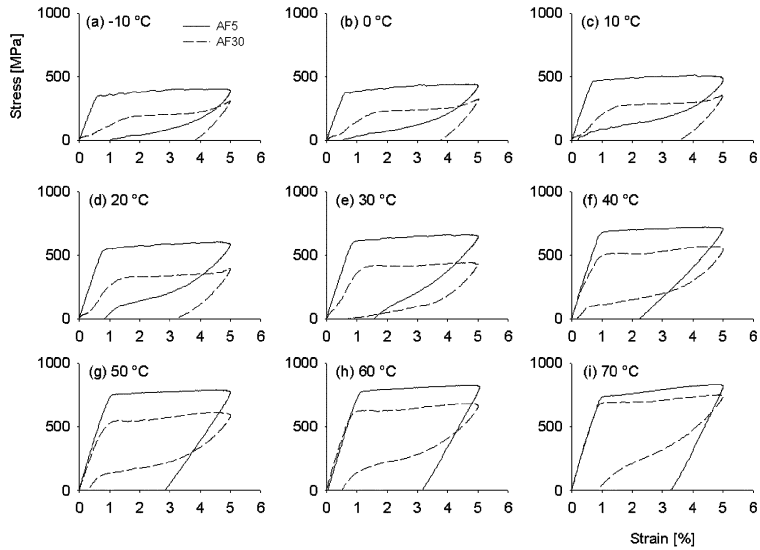


Fig. 3 Stress - strain curves for the AF5 and AF30 materials at various temperatures

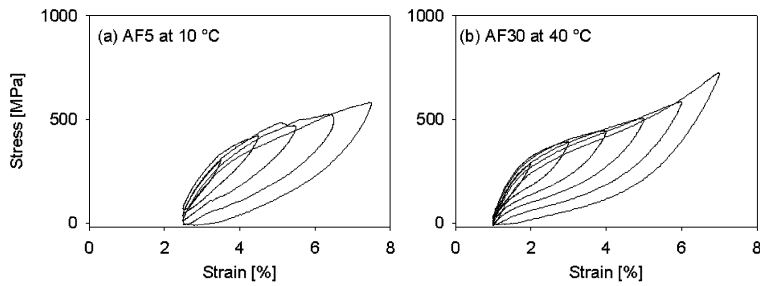


Fig. 4 Cyclic stress - strain curves for the AF5 and AF30 materials

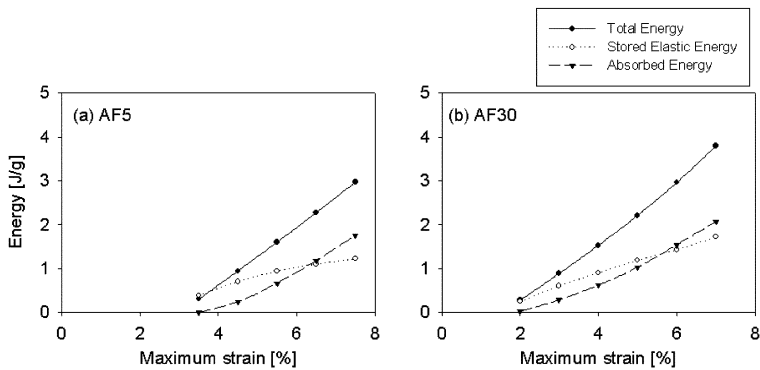


Fig. 5 Energy levels at varying strain amplitudes for the AF5 and AF30 materials

materials were pre-strained to avoid buckling of the wires during testing. 2.5% pre-strain for the AF5 material and 1% for the AF30 material. The wires were subjected to a 10 cycle training prior to testing. As the strain amplitude increases, the amount of energy absorbed increases for both materials. Fig. 5 shows the energy development as a function of maximum strain.

3. Constitutive models

Deformation of shape memory alloys are divided into two parts, elastic deformation of austenite or martensite and deformation caused by crystallographic transformations, i.e., transformation from austenite to martensite, or transformation between martensite variants. The deformation is dominated by the latter part, making transformation kinetics a governing factor. For this reason it is common to divide constitutive models into a mechanical part, to govern the stress-strain relations, and a kinetic part to govern the transformations. In the following, superscripts M' , M and A , denotes twinned martensite, detwinned martensite and austenite, respectively. Symbols σ_s and σ_f denotes critical stress for starting and finishing transformations, respectively.

3.1. Constitutive equation

Brinson (1993) developed a one dimensional constitutive model for SMA based on the work of Tanaka (1986) and Liang & Rogers (1997). The stress-strain relations are governed by the constitutive equation

$$\dot{\sigma} = D\dot{\varepsilon} + \Omega\dot{\xi} + \Theta\dot{T} \quad (1)$$

where $\dot{\sigma}$, $\dot{\varepsilon}$, $\dot{\xi}$ and \dot{T} are the time derivatives of stress, strain, martensite fraction and temperature, respectively. The parameter D represents the elasticity modulus, Ω the transformation tensor and Θ the thermo elastic tensor.

The original models of Tanaka and Liang & Rogers do not take into account the difference between stress induced martensite and thermally induced martensite.

Consequently their models can not describe SMA behaviour for temperatures below M_s (Brinson 1993). By separating the two types of martensite so that

$$\xi = \xi_s + \xi_T \quad (2)$$

where the subscripts “S” and “T” denotes stress induced and temperature induced martensite respectively, it is possible to describe the material behaviour in the temperature range $M_f < T < M_s$. Inserting Eq. (2) into Eq. (1) gives, after some calculations, an equation that is able to describe any behaviour for all temperatures:

$$\sigma - \sigma_0 = D(\varepsilon - \varepsilon_0) + \Omega(\xi_s - \xi_{s0}) + \Theta(T - T_0) \quad (3)$$

here the subscript “0” indicates initial values of the variables.

3.2. Kinetic relations

At temperatures $T \leq M_s$ the critical transformation stresses $\sigma_s^{M' \rightarrow M}$ and $\sigma_f^{M' \rightarrow M}$ are constant and may be treated as material constants (Brinson 1993). By combining this with the cosine model proposed by Liang & Rogers (1997), and the assumption $\xi = \xi_s + \xi_T$ one gets Brinson’s transformation equations for SMA:

$$\xi_s = \frac{1 - \xi_{SM}}{2} \cos \left\{ \frac{\pi}{\sigma_s^{M' \rightarrow M} - \sigma_f^{M' \rightarrow M}} [\sigma - \sigma_f^{M' \rightarrow M} - C_M(T - M_s)] \right\} + \frac{1 + \xi_{SM}}{2}. \quad (4)$$

The parameter C_M is a material constant and represents the slope in the critical stress – temperature curve ($C - T$ curve) for forward transformation. ξ_{SM} denotes the initial value of martensite fraction when transformation starts. Eq. (4) describes transformation from austenite to detwinned martensite. It is valid for temperatures $T \geq M_s$ and in the stress range

$$\sigma_s^{A \rightarrow M} = \sigma_s^{M' \rightarrow M} + C_M(T - M_s) < \sigma < \sigma_f^{M' \rightarrow M} + C_M(T - M_s) = \sigma_f^{A \rightarrow M}. \quad (5)$$

To describe transformation from twinned martensite to detwinned martensite the equation

$$\xi_S = \frac{1 - \xi_{SM}}{2} \cos \left\{ \frac{\pi}{\sigma_s^{M' \rightarrow M} - \sigma_f^{M' \rightarrow M}} (\sigma - \sigma_s^{M' \rightarrow M}) \right\} + \frac{1 + \xi_{SM}}{2} \quad (6)$$

is used. The above equation is valid for temperatures $T < M_s$ and

$$\sigma_s^{M' \rightarrow M} < \sigma < \sigma_f^{M' \rightarrow M}. \quad (7)$$

When $T > A_s$ no twinned martensite exists so that $\xi = \xi_S$. When mechanically unloading the material the so called reverse transformation from detwinned martensite to austenite will occur and can be described by the equation

$$\xi = \frac{\xi_M}{2} \{ \cos [a_A(T - A_s) - b_A \sigma] + 1 \} \quad (8)$$

ξ_M denotes the initial value of martensite and the parameters a_A and b_A are material parameters and are obtained from the previously defined material parameters, A_f , A_s and C_A ;

$$a_A = \frac{\pi}{A_f - A_s} \text{ and } b_A = -\frac{a_A}{C_A} \quad (9)$$

where C_A denotes the slope in the $C - T$ curve for reverse transformation. Eq. (8) is valid for

$$\sigma_s^{M \rightarrow A} = C_A(T - A_s) - \frac{\pi}{|b_A|} \leq \sigma \leq C_A(T - A_s) = \sigma_f^{M \rightarrow A} \quad (10)$$

Eqs. (5), (7) and (10) indicate the transformation strips for Brinson's model, i.e., the region between the critical stresses where transformation may occur (Tanaka 1986).

3.3. Effect of non-constant material parameters

Until now the elasticity modulus of the material during phase transformation has been assumed to be constant. In reality both the austenite and martensite phases exists and the elasticity modulus is dependent of the martensite fraction (Brinson 1993). To describe this Liang and Sato & Tanaka suggested the following rule of mixture (Brinson 1993)

$$D(\xi) = D_A + \xi(D_M - D_A) = D_A + D_{MA}\xi. \quad (11)$$

Differentiation with respect to ξ yields

$$D'(\xi) = D_{MA}. \quad (12)$$

The parameters D_A and D_M are the elasticity modulus for SMA when it is 100% austenite and 100% martensite, respectively. By combining Eqs. (3) and (11) a general expression for $\Omega(\xi)$, considering non-constant elasticity modulus, may be derived:

$$\Omega(\xi) = \frac{[\sigma - \sigma_0 - D(\xi)(\varepsilon - \varepsilon_0)]}{\xi - \xi_0} \quad (13)$$

In the above equation, the working temperature is considered constant so the term $\Theta\Delta T$ is zero for this derivation. Eq. (13) can easily be modified to consider the change of working temperature if necessary. Assuming forward transformation and letting ξ_{\max} denote a known value of the martensite fraction at a given level of deformation ε_{\max} , the stress σ_{\max} in this point can be calculated from Eq. (4) if the temperature is above M_s , or from Eq. (6) if the temperature is below M_s :

$$\sigma_{\max} = \left(\frac{\sigma_s^{M' \rightarrow M} - \sigma_f^{M' \rightarrow M}}{\pi} \right) \arccos[2\xi_{\max} - 1] + \sigma_{cr} \quad (14)$$

where σ_{cr} denotes $\sigma_f^{A \rightarrow M}$ if $T > M_s$ and $\sigma_f^{M' \rightarrow M}$ if $T < M_s$.

The starting stress σ_{\max} for any reverse transformation with arbitrary ξ_{\max} can be calculated from Eq. (8):

$$\sigma_{\max} = \left(\frac{1}{b_A} \right) \arccos[2\xi_{\max} - 1] - C_A(T - A_s). \quad (15)$$

The starting point of forward transformation and the end of reverse transformation have identical conditions: $\xi_0 = 0$, $\sigma_0 = \sigma_{\min}$ and $\varepsilon_0 = \varepsilon_{\min}$. A general expression from Eq. (13) which works for both forward and reverse transformation (to any degree of transformation) can be written:

$$\Omega(\xi) = \frac{[\sigma_{\max} - \sigma_{\min} - D(\xi)(\varepsilon_{\max} - \varepsilon_{\min})]}{\xi_{\max}}. \quad (16)$$

The derivative of Eq. (16) thus becomes:

$$\Omega'(\xi) = -\frac{D_{MA}(\varepsilon_{\max} - \sigma_{\min})}{\xi_{\max}}. \quad (17)$$

4. Analysis results

Numerical analyses are conducted on four different damper systems to predict the behaviour of seismic dampers containing composite NiTi-wires. The AF5 and AF30 materials presented in chapter 2 are used in the compositions. Olsen (2006) conducted a series of tests on the AF5 and AF30 materials, for a temperature range covering all phase transformation temperatures listed in Table 2. The objective of these tests was to establish material parameters for use in the numerical analyses of the dampers. The parameters are presented in Table 3. Here the transformation strain (ε_L) is introduced.

Each damper system consists of three parallel coupled wires and is exposed to a deformation controlled load cycle. The average stress is calculated using the Finite Element Method (FEM) with one dimensional truss elements; this is shown in Eq. (18).

Table 3 Material parameters for the AF5 and the AF30 material

Material	D_M [MPa]	D_A [MPa]	C_M [MPa/°C]	C_A [MPa/°C]	$\sigma_s^{M' \rightarrow M}$ [MPa]	$\sigma_s^{M \rightarrow M'}$ [MPa]	ε_L
AF5	14000	62188	8.03	7.34	72.72	296.86	0.0534
AF30	21784	56730	4.27	8.80	64.27	394.20	0.0466

$$\sigma_{avg} = \frac{\sum \sigma_i}{3}, \quad i = 1, 2, 3 \quad (18)$$

where σ_i represents the stress in each element. The dissipated energy is calculated through the integral

$$E_{dissipated} = \left(\int_0^{\varepsilon_{max}} \sigma(\varepsilon) d\varepsilon|_{loading} - \int_0^{\varepsilon_{max}} \sigma(\varepsilon) d\varepsilon|_{unloading} \right) V \quad (19)$$

which is approximated through the rectangular rule:

$$E_{dissipated} = \left(\sum_{n=0}^N \frac{1}{2} [\sigma_n + \sigma_{n+1}] \Delta\varepsilon|_{loading} - \sum_{n=0}^N \frac{1}{2} [\sigma_n + \sigma_{n+1}] \Delta\varepsilon|_{unloading} \right) V. \quad (20)$$

V is the volume of the body, and n is the increment number in the numerical simulations.

Three working temperatures are chosen to cover the temperature dependent properties PE and SME and three deformation levels are considered for each damper. The maximum strain for each cycle is chosen according to the martensite fraction of the AF5 wires. The control values are $\xi_{max}^{AF5} = 0.5$, $\xi_{max}^{AF5} = 0.75$ and $\xi_{max}^{AF5} = 1$. Martensite fraction in the AF30 wires will differ due to a shorter transformation strain ε_L . Table 4 shows the maximum strain for each level and temperature.

In Table 5 it can be seen which temperature dependent effects are present in the different damper systems at the different temperatures. At $T < A_f^{AF5} < A_f^{AF30}$ the wires experience SME and partial PE, when $A_f^{AF5} < T < A_f^{AF30}$ both SME and PE are present, while when $A_f^{AF5} < A_f^{AF30} < T$ all wires exhibits PE. springs, dashpots and spring-dashpot combinations are used to represent pseudoelasticity (PE), shape memory effect (SME) and the PE-SME combination respectively. SME is used to describe the apparent plastic deformation in the wires.

4.1. Damper 1

Damper 1 is composed of three AF5 wires. Fig. 6 shows the stress–strain curves of damper 1. The average critical stresses where forward transformation starts ($\sigma_{cr}^{A \rightarrow M}$) are 382 MPa at $T = 0$ °C, 544 MPa at $T = 25$ °C and 700 MPa at 45 °C. The amount of energy is plotted against temperature in

Table 4 Deformation levels for each working temperature

Temperature	ξ_{max}^{AF5}	$\varepsilon_{max} (\xi_{max}^{AF5} = 0.5)$	$\varepsilon_{max} (\xi_{max}^{AF5} = 0.75)$	$\varepsilon_{max} (\xi_{max}^{AF5} = 1)$
0 °C		3.25 %	4.60 %	6.00 %
25 °C		3.55 %	4.90 %	6.20 %
45 °C		3.80 %	5.10 %	6.45 %

Table 5 Systems and working temperatures considered in the study

Temperature	Damper 1	Damper 2	Damper 3	Damper 4
0 °C				
25 °C				
45 °C				

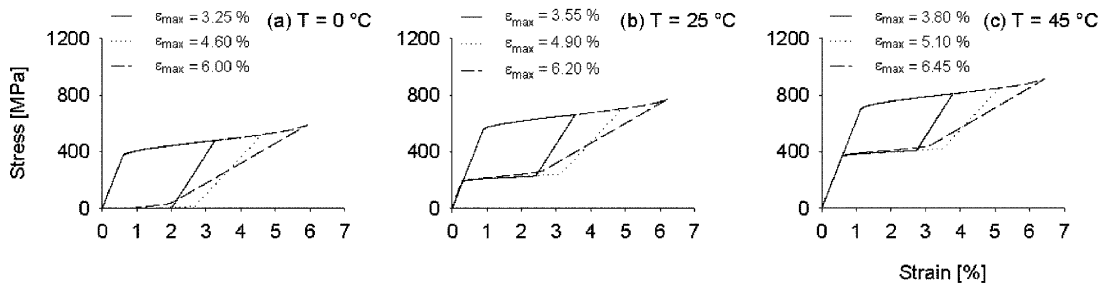


Fig. 6 Stress - strain curves for Damper 1 at different temperatures (a) $T=0$ °C, (b) $T=25$ °C, (c) $T=45$ °C

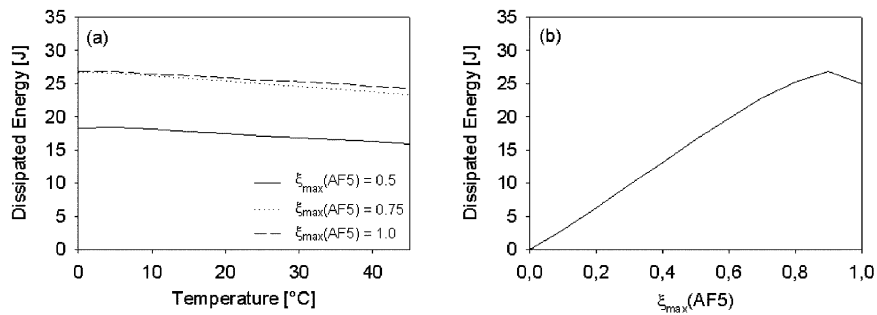


Fig. 7 Dissipated energy as a function of (a) temperature and (b) ξ_{max}^{AF5}

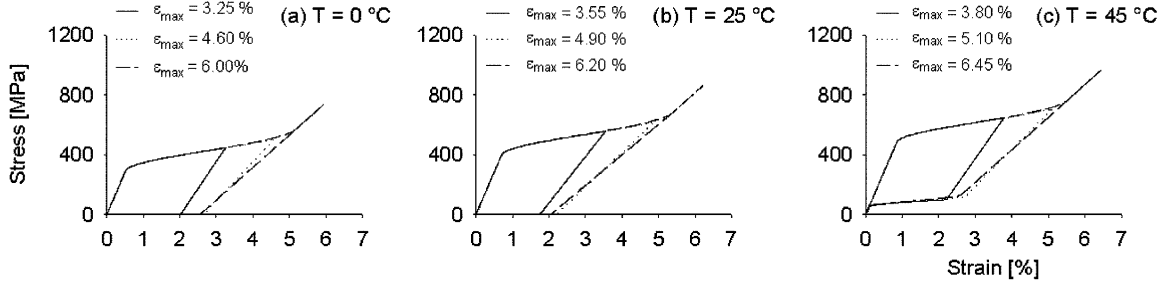


Fig. 8 Stress - strain curves for Damper 2 at different temperatures (a) $T=0$ °C, (b) $T=25$ °C, (c) $T=45$ °C

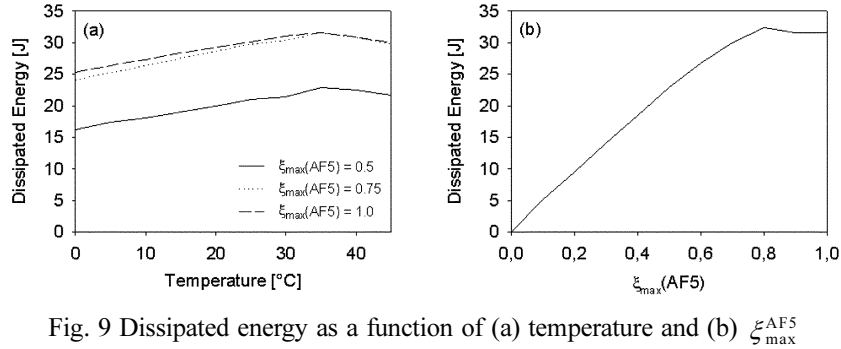


Fig. 9 Dissipated energy as a function of (a) temperature and (b) $\zeta_{\max}^{\text{AF5}}$

Fig. 7(a). It is interesting to note that the energy dissipated decreases linearly with the temperature from $T=0$ °C. The dissipation energy decreases is of 13%, 13% and 9% at $T=0$ °C to 45 °C when $\zeta_{\max}^{\text{AF5}} = 0.5$, $\zeta_{\max}^{\text{AF5}} = 0.75$ and $\zeta_{\max}^{\text{AF5}} = 1$, respectively. When increasing the martensite control value from $\zeta_{\max}^{\text{AF5}} = 0.5$ to $\zeta_{\max}^{\text{AF5}} = 0.75$ the energy dissipated increases accordingly, but when increasing additionally to $\zeta_{\max}^{\text{AF5}} = 1$ there is little change in the energy level. This effect can mainly be explained by the change in the elasticity modulus as the forward transformation evolves. Fig. 7(b) show the dissipated energy plotted against $\zeta_{\max}^{\text{AF5}}$. The level of energy dissipation increases linearly until $\zeta_{\max}^{\text{AF5}} \approx 0.8$ and peaks at 26.89 J when $\zeta_{\max}^{\text{AF5}} = 0.9$.

4.2. Damper 2

Damper 2 which consists of three AF30 wires exhibits a similar behaviour to Damper 1. The stress, however, is lower than that of Damper 1 (see Fig. 8). The critical stresses where transformation starts ($\sigma_{cr}^{A \rightarrow M}$) are 286 MPa at 0 °C, 414 MPa at 25 °C and 477 MPa at 45 °C. In this case the energy dissipation increases linearly from $T=0$ °C until its maximum at $T=35$ °C, which lies between A_s and A_f , and decreases linearly after the peak (Fig. 9a). Also for this damper there is an upward shift in the amount of energy dissipated when altering the martensite control value from $\zeta_{\max}^{\text{AF5}}=0.5$ to $\zeta_{\max}^{\text{AF5}}=0.75$ and nearly no difference between the two cases $\zeta_{\max}^{\text{AF5}}=0.75$ and $\zeta_{\max}^{\text{AF5}}=1$. But since maximum martensite fraction for AF30 is approximately 0.9 when $\zeta_{\max}^{\text{AF5}}=0.75$ the transformation strain is approximately equal for the two latter load cases. Fig. 9(b) shows the of dissipated energy as a function of $\zeta_{\max}^{\text{AF5}}$. The energy level increases approximately linearly up to its maximum 32.32 J at $\zeta_{\max}^{\text{AF5}}=0.8$ before it decrease slightly towards $\zeta_{\max}^{\text{AF5}}=1$.

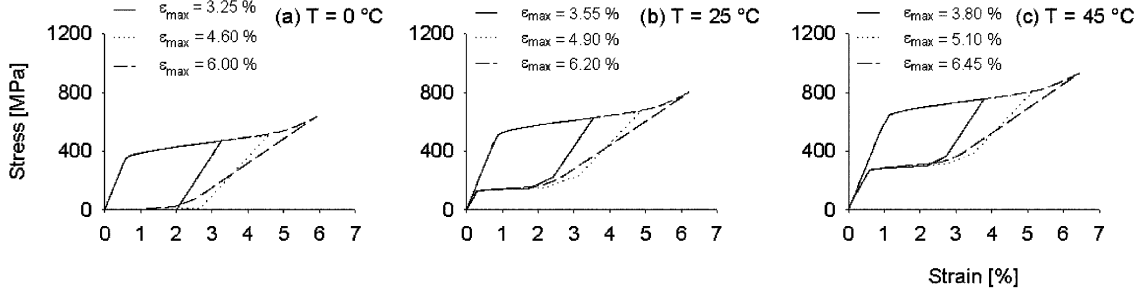


Fig. 10 Stress - Strain curves for Damper 3 at different temperatures (a) $T=0$ °C, (b) $T=25$ °C, (c) $T=45$ °C

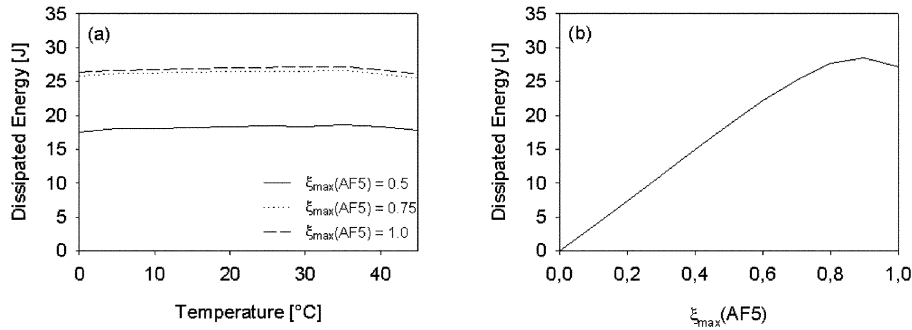


Fig. 11 Dissipated energy as a function of (a) temperature and (b) $\frac{\varepsilon_{\max}^{\text{AF5}}}{\zeta_{\max}^{\text{AF5}}}$

4.3. Damper 3

Damper 3 is a composite damper which consists of two AF5 wires and one AF30 wire. When combining different materials in a parallel damper configuration the properties of the material which is represented with most wires will dominate the damper behaviour of the damper. At $T = 0$ °C a combination of SME and PE-SME is present and from Fig. 10(a) it can be seen that some degree of spring-back is present in the damper. This effect is due to the PE-SME combination in the AF5-wires at this temperature. At $T = 25$ °C and $T = 45$ °C the damper experience complete PE which can be ascribed to the two AF5-wires and all three wires respectively (see Fig. 10b and Fig. 10c). When damper deformation is controlled by the condition $\frac{\varepsilon_{\max}^{\text{AF5}}}{\zeta_{\max}^{\text{AF5}}} = 1$, there is a break in the curve at the end of the upper plateau (see Fig. 10). This break is due to the linear deformation of the AF30-wire in the damper configuration after the transformation is finished. The average critical stresses where forward transformation starts ($\sigma_{cr}^{A \rightarrow M}$) are 350 MPa at $T = 0$ °C, 499 MPa at $T = 25$ °C and 626 MPa at $T = 45$ °C. The dissipated energy for this damper configuration is nearly constant in the temperature range 0 °C - 35 °C before it decreases slightly when $T > 35$ °C (see Fig. 11a). From Fig. 11(b) it can be observed that the level of dissipated energy increases linearly with $\frac{\varepsilon_{\max}^{\text{AF5}}}{\zeta_{\max}^{\text{AF5}}}$ when $\frac{\varepsilon_{\max}^{\text{AF5}}}{\zeta_{\max}^{\text{AF5}}} < 0.7$. The curve flattens slightly from $\frac{\varepsilon_{\max}^{\text{AF5}}}{\zeta_{\max}^{\text{AF5}}} = 0.7$ until its peak value 28.44 J, at $\frac{\varepsilon_{\max}^{\text{AF5}}}{\zeta_{\max}^{\text{AF5}}} = 0.9$, before it decreases.

4.4. Damper 4

Fig. 12 shows the stress-strain curves for damper 4, which is composed of one AF5-wire and two AF30-wires. At $T = 0$ °C a residual strain is present in the damper, and some level of reverse

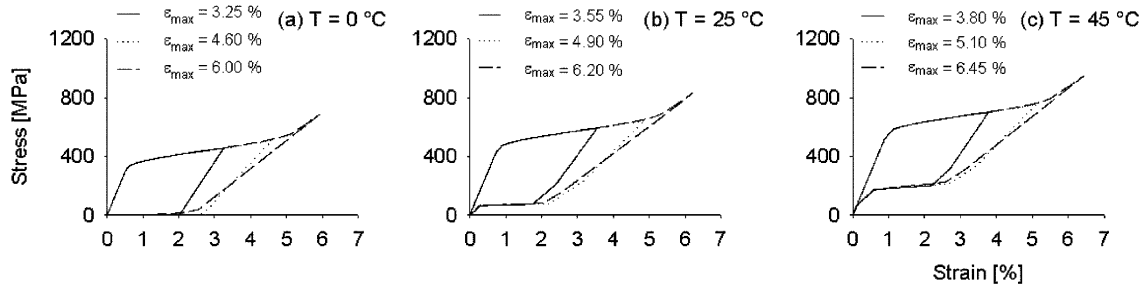


Fig. 12 Stress - Straincurves for Damper 4 at different temperatures (a) $T=0$ °C, (b) $T=25$ °C, (c) $T=45$ °C

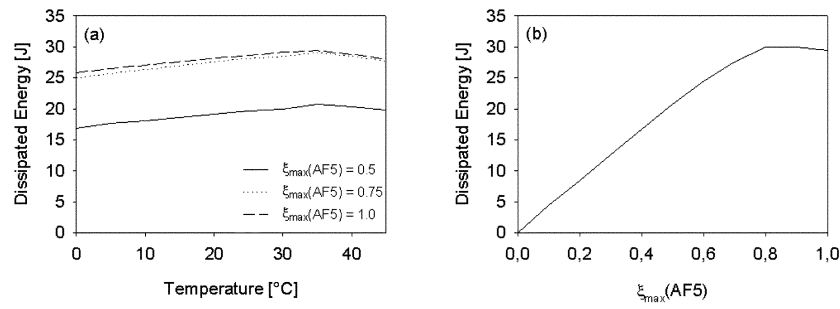


Fig. 13 Dissipated energy as a function of (a) temperature and (b) ζ_{max}^{AF5}

transformation occur at this temperature (see Fig. 12a). At $T = 25$ °C and $T = 45$ °C the damper experience complete PE which can be ascribed to the AF5-wire and all three wires respectively. The break in the curve on the upper plateau for the load case $\zeta_{max}^{AF5}=1$, is a consequence of the AF30 transformation strain being shorter than the AF5 transformation strain, thus leading to linear deformation of the AF30-wire (see Fig. 12c). The average critical stresses $\sigma_{cr}^{A \rightarrow M}$ where forward transformation starts are 318 MPa at $T=0$ °C, 456 MPa at $T=25$ °C and 552 MPa at $T=45$ °C. The energy dissipation, for the current damper configuration, increases with temperature up to 35 °C where the maximum value is reached and decreases for temperatures above 35 °C (see Fig. 13a). The effect of changing the martensite control value on the level of dissipated energy is plotted in Fig. 13(b). A linear increase in energy dissipation is evident until $\zeta_{max}^{AF5} = 0.8$ is reached.

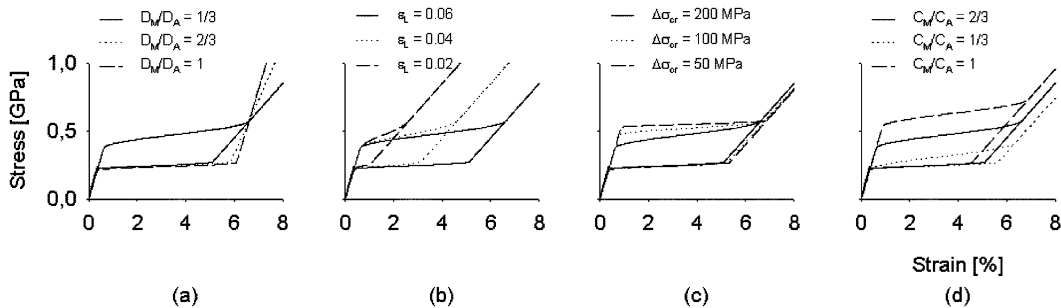


Fig. 14 Stress - strain curves showing the effect of changing (a) elasticity modulus, (b) transformation strain, (c) critical transformation stress and (d) C_M/C_A - ratio

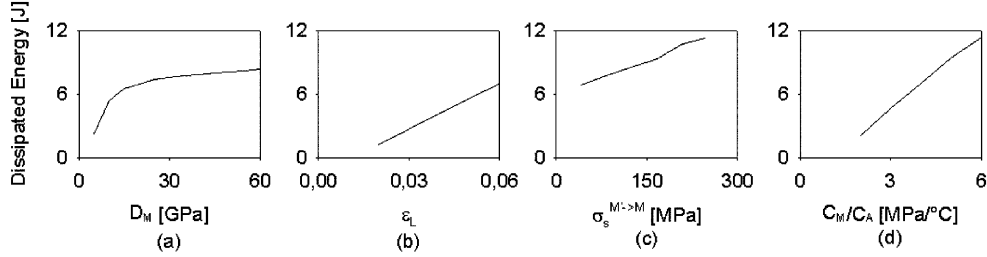


Fig. 15 Effect on dissipated energy of changing (a) elasticity modulus, (b) transformation strain, (c) critical transformation stress and (d) C_M/C_A - ratio

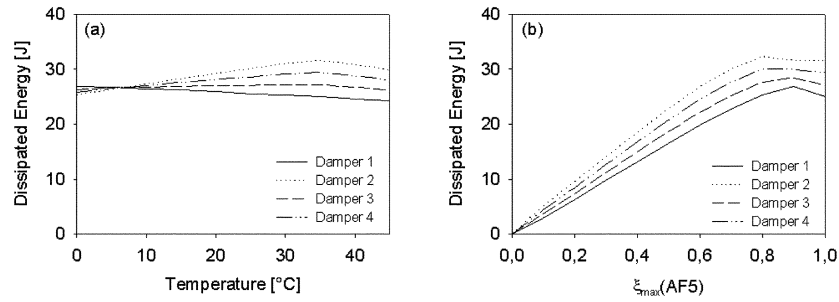


Fig. 16 Comparison of dissipated energy for the different dampers (a) as a function of temperature and (b) as a function of ξ_{\max}^{AF5}

4.5. Parameter study

In this section the effect of the key damper material parameters is investigated. The simulations are conducted on a single wire at 45 °C. A total elongation of 10% is applied to make sure that complete transformations are achieved in all simulations. The parameters studied are: the elasticity modulus, forward transformation strain (ε_L), critical stresses ($\Delta\sigma^{M' \rightarrow M} = \Delta\sigma_f^{M' \rightarrow M} - \sigma_s^{M' \rightarrow M}$) and the slopes of the C - T curves, C_M and C_A . Values used for these parameters cover a wide range of commercially available NiTi-alloys.

Fig. 14(a) and Fig. 15(a) show the effect of altering the martensite elasticity modulus D_M . The austenite elasticity modulus is kept constant in this study. The results show that a decrease in D_M from 60000 MPa to 20000 MPa leads to a drop in energy dissipation of 16% (Fig. 15a). It also results in a shortening of the reverse transformation strain (lower plateau in Fig. 14a). From Fig. 15(a) it is interesting to note that the level of dissipated energy increases rapidly up to $D_M \approx 10000$ MPa, and slowly increases toward $D_M = D_A$. Changing the transformation strain, ε_L , pose great significance on the damper behaviour. The size of these loops is strongly influenced this parameter, as can be seen in Fig. 14(b). There is a drop of 82% in dissipated energy, when changing ε_L from 0.06 to 0.02 (see Fig. 15b). Fig. 14(c) displays the stress-strain curves for the case of changing $\sigma_s^{M' \rightarrow M}$. In all the analyses the critical stress $\sigma_f^{M' \rightarrow M}$ is kept constant as 250 MPa. There is an upward shift in the transformation plateau as $\sigma_s^{M' \rightarrow M}$ increases. This leads to an increase in dissipated energy of 32%. From Fig. 15(c) it can be observed that the dissipated energy increase linearly with $\sigma_s^{M' \rightarrow M}$ until $\sigma_s^{M' \rightarrow M} = 125$ MPa, after that the curve then takes on a slightly S-shaped form. Fig. 14(d) displays the effect of C_M . C_A is kept constant at 6 MPa/°C and C_M is altered in such a way that the $C_M - C_A$ ratio is 1/3, 2/3 and 3/3. Altering

C_M has a significant effect on the stress-strain response; the upper transformation plateau shifts upward while the reverse transformation strain shortens when C_M is increased. The difference in dissipated energy between the cases $C_M/C_A = 1$ and $C_M/C_A = 1/3$ is 82%. From Fig. 15(d) it may be seen that the energy dissipation is increasing linearly with C_M .

5 Discussions and summary

A seismic damper's primary task is to repeatedly dissipate energy subjected to a structure during seismic activity. In a shape memory alloy based damper this means that the material must be able to sustain multiple loads without losing its dissipation capabilities. The AF5 and AF30 materials tested in this work produced unwanted residual strain during testing. This unwanted effect is probably due to stress concentrations around the largest inclusions, which agrees well with observations made on steel, where inclusions larger than 10 μm are detrimental to the material behaviour (Atkinson and Shi 2003). The inclusions observed here are less than 10 μm but may influence the behaviour since the stress concentrations around them can nucleate martensite during loading. The presence of residual strain also deteriorates the re-centring capabilities of the materials. To circumvent the residual strain, the wires have to be trained and pre-strained. A 10 cycle training leads to losses in energy absorption of 21% and 6% for the AF5 and AF30 materials, respectively, compared to the absorption levels of wires in untrained condition.

In order to optimize damper design, numerical analyses are vital. The numerical analyses made in this work, showed that the composition of the damper materials influences the damper's dissipation capabilities. Fig. 16a compares the energy absorption levels of the different dampers. The figure shows that dampers with homogenous wires experience the highest dissipation level at temperatures between A_s and A_f . Within this temperature range, however, residual strain will be present reducing the dampers re-centring capabilities. This implies that it is desirable to use materials which experience pseudoelasticity when functioning in any working temperature, i.e., in this case, the AF5 material. However, Fig. 16(a) also shows that the damper with homogenous AF30 wires exhibit the best dissipation capabilities, but since AF30 has a A_f of 41 °C the re-centring capabilities are limited to high temperatures only. This indicates that to ensure re-centring and desired dissipation, a balance between material types has to be employed. Fig. 16(b) shows the variation of energy dissipation as a function of $\zeta_{\sigma_{\max}}^{\text{AF5}}$. The energy level reaches its maximum in the range $0.8 < \zeta_{\sigma_{\max}}^{\text{AF5}} < 0.9$, which indicates that it is not optimal to let the wires be deformed until complete martensite transformation has occurred.

5.1. Summary

As a part of the EU-supported project, WIND-CHIME, two NiTi-alloys have been experimentally tested and characterized both metallurgical and mechanical. In addition, design principles for a new damper system have been proposed and numerically investigated. The studies show that the two alloys may be used in a damper if precautions, such as pre-straining and training, are made. However, the alloys exhibit unwanted residual strain when exposed to a 5% elongation. The two particular alloys are therefore not considered to be ideal in a seismic damper.

The numerical investigations of the new damper system show that when employing two different materials in a damper, the material with highest A_f should dominate the damper configuration. Such a configuration exhibits the highest energy dissipation level for the working temperature range used in

this study. The parameter study shows that the material parameters have a great effect on the damper behaviour, thus being of great importance in the material selection process.

References

- Atkinson, H. V. and Shi, G. (2003), "Characterization of inclusions in clean steels: a review including the statistics of extreme methods", *Progress in Materials Science*, **48**(5), 457-520.
- Aurichio, F., Faravelli, L., Magonette, G. and Torra, V. (2001), *Shape Memory Alloys. Advances in Modelling and Applications*, International Center for Numerical Methods in Engineering (CIMNE), Barcelona, Spain.
- Brinson, L. C. (1993), "One-dimensional constitutive behavior of shape memory alloys: Thermomechanical derivation with non-constant material functions and redefined martensite internal variable", *J. Intelligent Material Sys. Struct.* **4**(2), 229-242.
- Clark, P. W., Aiken, I. D., Kelly, J. M., Higashino, M. and Krumme, R. (1995), "Experimental and analytical studies of shape-memory alloy dampers for structural control", *Proceedings of SPIE - The International Society for Optical Engineering*, San Diego, Mars.
- Dolce, M., Cardone, D. & Marnetto, R. (2001), "SMA recentering devices for seismic isolation of civil structures", *Proceedings of SPIE - The International Society for Optical Engineering*, Newport Beach, Mars.
- Duerig, T. W., Ed. (1990), *Engineering Aspect of Shape Memory Alloys*, Butterworth-Heinemann Ltd., London, UK.
- Funakubo, H., Ed. (1987), *Shape memory alloys. (Precision and robotics, Vol. 1)*, Gordon and Breach science publishers, New York, NY.
- Han, Y. L., Xing, D. J., Xiao, E. T. and Li, A. Q. (2005), "NiTi-wire shape memory alloy dampers to simultaneously damp tension, compression, and torsion", *J. Vib. Control* **11**(8), 1067-1084.
- Janke, L., Czaderski, C., Motavalli, M. and Ruth, J. (2005), "Applications of shape memory alloys in civil engineering structures - Overview, limits and new ideas", *Mater. Struct.* **38**(279), 578-592.
- Liang, C. and Rogers, C. A. (1997), "One-dimensional thermomechanical constitutive relations for shape memory materials (Reprinted from Journal of Intelligent Material Systems and Structures, vol 1, pg 207-234, 1990)", *J. Intelligent Mater. Sys. Struct.*, **8**(4), 285-302.
- Olsen, J. S. (2006), "Seismic dampers with composite NiTi-wires – A new damper system", M.Sc. Thesis, Norwegian University of Science and Technology (NTNU), Unpublished, Trondheim.
- Saadat, S., Salichs, J., Noori, M., Hou, Z., Davoodi, H., Bar-On, I., Suzuki, Y. and Masuda, A. (2002), "An overview of vibration and seismic applications of NiTi shape memory alloy", *Smart Mater. Struct.*, **11**(2), 218-229.
- Tanaka, K. (1986), "A thermomechanical sketch of shape memory effect - one-dimensional tensile behavior", *Res. Mechanica*, **18**(3), 251-263.